Tailoring Terahertz Near-Field Enhancement via Two-Dimensional Plasmons

Arthur R. Davoyan,[1,2] Vyacheslav V. Popov,[1,2] and Sergei A. Nikitov[2,3]

[1]*Kotelnikov Institute of Radio Engineering and Electronics (Saratov Branch), Russian Academy of Sciences, Zelenaya 38, Saratov 410019, Russia*

[2]*Saratov State University, Astrakhanskaya 83, Saratov, 410012, Russia*

[3]*Kotelnikov Institute of Radio Engineering and Electronics, Russian Academy of Sciences, Mokhovaya 11-7, Moscow, 125009, Russia*

(Received 4 October 2011; published 19 March 2012)

We suggest a novel possibility for electrically tunable terahertz near-field enhancement in flatland electronic materials supporting two-dimensional plasmons, including recently discovered graphene. We employ electric-field effect modulation of electron density in such materials and induce a periodic plasmonic lattice with a defect cavity. We demonstrate that the plasmons resonantly excited in such a periodic plasmonic lattice by an incident terahertz radiation can strongly pump the cavity plasmon modes leading to a deep subwavelength concentration of terahertz energy, beyond $\lambda/1000$, with giant electric-field enhancement factors up to 10^4, which is 2 orders of magnitude higher than achieved previously in metal-based terahertz field concentrators.

DOI: 10.1103/PhysRevLett.108.127401 PACS numbers: 85.60.−q, 07.57.−c, 42.25.Bs, 42.79.Pw

Many material properties are sensitive to terahertz (THz) radiation, which makes THz spectroscopy an essential tool for the analysis of material microstructure, chemical composition, and for medical treatment [1,2]. However, the diffraction limit of conventional optical systems, i.e., their inability to focus light in deep subwavelength regime, challenges the study of individual micro- and nanostructures.

Recent works have extensively discussed concentration of the THz energy beyond the diffraction limit with metallic structures, including, nanoapertures [3], tapers [4–6], and metal edges [7]. In particular, in Refs. [4,5] it was shown that tapered metallic rods and wedges can focus THz and midinfrared radiation into nanometer-size spots. In Ref. [8], THz energy concentration in a metallic nanoslit beyond the skin-depth limit was demonstrated with the field enhancement factors up to 10^3 at 0.1 THz, nevertheless, the effect was steeply decreasing with frequency increase down to field enhancement factors 100 at frequencies higher than 1 THz. One of the key approaches for the design and study of the metallic nanostructures for THz photonics is making parallels with optical plasmonics. However, at THz frequencies the electromagnetic field is weekly localized near the metal interface and can be confined only between closely placed metallic surfaces or in dispersion-engineered geometries [9,10]. Efficient coupling of THz radiation into the metallic nanostructures demands comprehensive antenna design, which, together with the lack in tunability, makes the development of functional integrated THz photonic devices based on metallic nanostructures a challenging task.

Employing structures supporting intrinsic two-dimensional (2D) plasmons, i.e., waves of free electron density physically localized in a plane, may resolve these problems and change significantly the design principles of THz photonic devices. Among such structures are semiconductor quantum wells, supporting 2D electron gases, and recently discovered graphene [11], a natural two-dimensional material. Contrary to metal structures, the electronic properties of such materials, and particularly conductivity, can be easily tuned by using the electric-field effect, i.e., the material's electron concentration can be varied significantly when the material is subjected to a static electric potential [11]. The electric-field effect was utilized for the development of compact tunable THz sources and detectors based on the field-effect transistors (FET), structures with a two-dimensional electron system loaded by gate electrodes [12,13]. In particular, it was shown that a FET with a periodic grating gate creates a periodic potential for 2D plasmons, leading to the resonant excitation of so-called 2D lattice plasmons [14–16]. Graphene has also attracted much attention for photodetection applications [17,18] and its potential prospects for THz photonics are currently an active research field [19–21]. However, to the best of our knowledge, THz field concentration and its enhancement in such 2D plasmonic structures has not been discussed yet.

In this Letter, we propose a novel mechanism for tunable THz near-field enhancement in structures with flatland electronic materials, supporting 2D plasmons. We modulate the electron concentration and corresponding 2D conductivity in such systems by applying an electric-field effect, and induce a periodic potential with a defect for 2D plasmons supported by such electronic materials. We analyze the excitation of the lattice and the cavity plasmons, and demonstrate that their interaction leads to a dramatic THz near-field enhancement, with giant field enhancement factors exceeding those observed previously in metal-based THz energy concentrators by 2 orders of magnitude. Finally, we show that the predicted effect can be observed in the entire THz frequency domain.

We study plasmon excitation in the FET structure with a split-grating gate, where the central gate finger is biased independently from the rest of the grating gate, see Fig. 1. We assume that a THz plane wave, with electric field perpendicular to the grating-gate fingers, $\mathbf{E}\|\mathbf{x}$, is incident normally upon the structure as shown schematically in Fig. 1. A periodic metallic grating with period L and gate finger width a is placed on the top of a dielectric substrate with permittivity ε, Fig. 1. We suppose that a 2D electron gas with the electron density N_0 is formed at distance h below the grating gate. Note that here, as an example, we consider a "conventional" 2D electron gas formed in a quantum well of semiconductor heterostrutures (GaAs/AlGaAs); such a choice is determined by currently developed experimental facilities for semiconductor based FETs. However, properties of graphene in a good approximation coincide with those of 2D electron gases [11,22–24]; therefore, the analysis developed in this Letter is applicable to the study of graphene based structures and the effects predicted here will be observed in corresponding graphene based FETs.

Negative electric potential applied to the central gate finger depletes the 2D electron concentration under this particular finger, see the inset to the Fig. 1. Therefore, the biased area acts as a tunable plasmonic cavity (defect) in a periodic plasmonic lattice. Note that the grating gate, if biased, creates a periodic modulation of electron concentration in the 2D electron channel, and hence the resonance frequency of the lattice plasmons can be also changed. Here, without loss of generality, we consider that the grating gate is not biased and the 2D electron density in the grating gated regions of the channel, N_0, remains homogeneous.

When the frequency of the incident THz wave ω is far away from the lattice resonances, the lattice plasmons cannot be excited and the 2D channel response is governed mainly by the Drude background conductivity. In this case, neglecting the excitation of the lattice plasmons, the plasmonic cavity can be fairly well modeled by a homogeneous 2D electron system gated only by a single gate

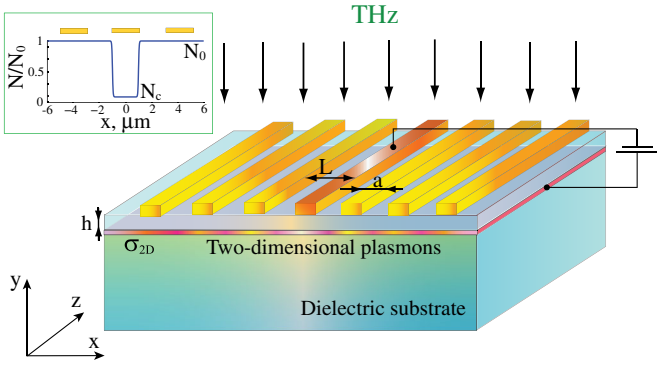

FIG. 1 (color online). Schematic of the split-grating-gate field-effect transistor, where the central gate contact is biased individually. The inset shows an example of the concentration profile in the channel.

finger. This system was analyzed in detail in Ref. [25], where it was shown that the cavity resonance frequencies roughly satisfy a simple electrostatic formula

$$\omega_{\mathrm{def}}^{(k)} = \sqrt{\frac{N_c e^2 h}{m^* \varepsilon_0 \varepsilon}} \frac{\pi k}{a + 2h}, \tag{1}$$

where k is the number of the resonance order, $m^* = 0.067m$ is the effective electron mass, and N_c is 2D electron density in the cavity.

In Fig. 2(a), we plot the dispersion of the cavity resonance frequency defined by Eq. (1) for four cavity modes with the variation of electron density in the biased area of the channel. Note that here we consider that $L = 4$ μm, $a = L/2$, $h = 200$ nm, $N_0 = 2.5 \times 10^{11}$ cm^{-2}, $\varepsilon = 12.8$. In the same figure, we mark the position of the fundamental resonance of the 2D lattice plasmon, calculated for a simple periodic FET. According to Fig. 2(a) the dispersions of the higher-order cavity resonances cross the lattice plasmon lattice resonance dispersion with depletion of the cavity concentration. In this case, we expect strong interaction between the cavity and the lattice plasmon modes.

To prove our predictions, we perform comprehensive numerical simulations using the commercial COMSOL multiphysics finite element method. We perform 2D simulations, considering no variation of the field in the $\mathbf{z}$ direction and searching for the field profiles in the (x-y) plane. Taking into account that the thickness of metal gate contacts is 4 orders of magnitude smaller than the incident wavelength (typically 100–300 nm), and that small skin depth prevents THz field penetration inside them, we approximate the grating gate by the sequence of infinitely thin perfect electric conductors. To model the structure, we use the supercell approximation Ref. [26]. In this method, we embed our structure of interest into a large supercell periodically repeated in the $\mathbf{x}$ direction. We consider that the supercell contains the defect and 36 periods of the grating gate on either side of it. Since the thickness of the typical quantum well is 10–30 nm and the electron motion is confined to the plane, the electromagnetic response of 2D electron gas in a local approximation can be described by the 2D Drude conductivity, $\sigma_{2D}(\omega) = N(x)e^2\tau/m^*(1 - j\omega\tau)$, where τ is the electron scattering time, $N(x) = (N_0 - N_c)[1 + 1/2\sum_{k=1}^{2} i^{2k} \tanh(\chi(x + i^{2k-2}a/2))] + N_c$ is the 2D electron density, here χ is a parameter responsible for smooth concentration transition near the cavity edges, see the inset to Fig. 1.

We introduce the cavity excitation factor as a ratio between the THz power absorbed in the cavity and the energy flux in the incident THz wave, $F = \mathrm{Re}(\int_{\mathrm{defect}} \sigma |E_x|^2 dx)/(2aP_{\mathrm{in}})$. First, we demonstrate the validity of our approach for the prediction of the cavity resonance positions. Using Eq. (1) and Fig. 2(a), we choose the depletion ratio $N_c/N_0 = 0.12$ in such a way that the third and the fourth cavity resonances are relatively close to the lattice plasmon resonance. We plot the spectrum of

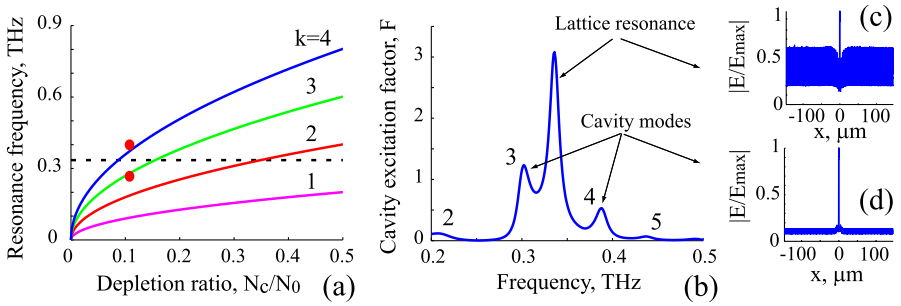

FIG. 2 (color online). (a) Plasmonic cavity resonance frequency as a function of 2D electron density under the defect gate for four cavity modes. The dashed line shows the position of the lattice plasmon resonance. Dots mark the positions of the third and fourth order cavity resonances shown in panel (b). (b) Cavity excitation factor spectrum for the cavity depletion ratio $N_c/N_0 = 0.12$. Numbers indicate the resonance orders. (c),(d) The mode profiles at the lattice resonance ($\omega = 0.336$ THz) and at the fourth order cavity plasmon resonance ($\omega = 0.388$ THz), respectively.

the cavity excitation factor for this case in Fig. 2(b). To identify the excited plasmon modes at each resonance, we analyze corresponding electric-field profiles, see Figs. 2(c) and 2(d). The analytically predicted positions of the lattice and the cavity resonances coincide reasonably well with the results of numerical simulations, see Fig. 2(a). The resonances of the cavity modes with the eigenfrequencies close to the lattice plasmon resonance frequency become stronger due to the strong intermode interaction, whereas the cavity modes are negligibly weak far away from the lattice plasmon resonance.

Moving further, we study the interaction between the lattice and the cavity plasmon modes. The cavity plasmon resonances are shifted to lower frequencies for a decreasing depletion ratio, see Fig. 2. For the depletion ratio $N_c/N_0 \simeq 0.1$ the fourth order cavity resonance merges with the lattice plasmon resonance leading to the increase of the resonance amplitude, see Fig. 3(a). For even smaller N_c/N_0, the resonances are separated again decreasing in amplitude, until the fifth cavity resonance approaches the lattice eigenfrequency. In Fig. 3(b), we plot the positions of the cavity resonances as functions of the depletion ratio showing the interaction between the cavity plasmon modes and the lattice plasmon mode. When the cavity and the lattice plasmon resonances approach each other, they experience strong interaction leading to the avoided crossing of corresponding resonances.

The observed dynamics can be qualitatively modeled by a system of two coupled linear oscillators, where the first oscillator corresponds to the lattice plasmon mode, being excited by the incident THz radiation, and the other corresponding to the plasmonic cavity, being pumped by the lattice mode only:

$$\ddot{x}_1 + 2\gamma_1\dot{x}_1 + \omega_{0,1}^2 x_1 = Ae^{j\omega t},$$
$$\ddot{x}_2 + \left(2\gamma_2 + \frac{C}{\omega_{01}^2 - \omega^2 + 2j\gamma_1\omega}\right)\dot{x}_2 + \sum \omega_{k,2}^2 x_2 = Bx_1, \quad (2)$$

where oscillator eigenfrequencies $\omega_{k,i}$ are determined from the resonance positions of corresponding unperturbed plasmon states, the decay factors γ_i can be estimated by the resonances' Q factors, A is the coupling constant between the incident radiation and the lattice plasmon mode, B is the coupling factor between the lattice plasmon mode and the cavity plasmon mode. Note that we have also accounted for the radiative damping of the cavity oscillator into the lattice mode [14,25]. We have solved the system Eq. (2) with appropriately chosen parameters B and C and found out that this simple model in a very good approximation describes the observed dynamics (not shown here).

In Figs. 4(a) and 4(b) we plot the electric-field enhancement factor, $|\mathbf{E}/\mathbf{E}_0|$ and the map of the electric-field distribution in the (x-y) plane in the avoided crossing regime for $N_c/N_0 = 0.1$ and $\omega = 0.332$ THz. The electric field is greatly enhanced in the cavity up to 150. The

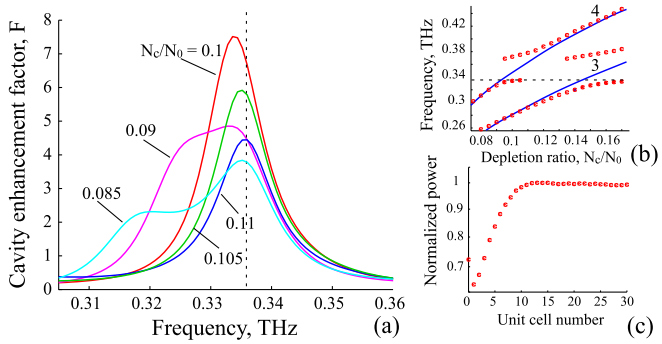

FIG. 3 (color online). (a) Cavity excitation factor spectrum for different depletion ratios, N_c/N_0. The dashed line shows the position of the unperturbed lattice plasmon resonance. (b) Dispersions of the third and fourth cavity resonances as functions of the cavity depletion ratio. Solid curves show the dispersion of corresponding unperturbed cavity modes. The dashed line marks the position of the unperturbed lattice plasmon resonance. (c) The power absorbed in a unit cell of the plasmonic lattice with increasing the lateral distance from the cavity (the power absorbed by the cavity is not featured here).

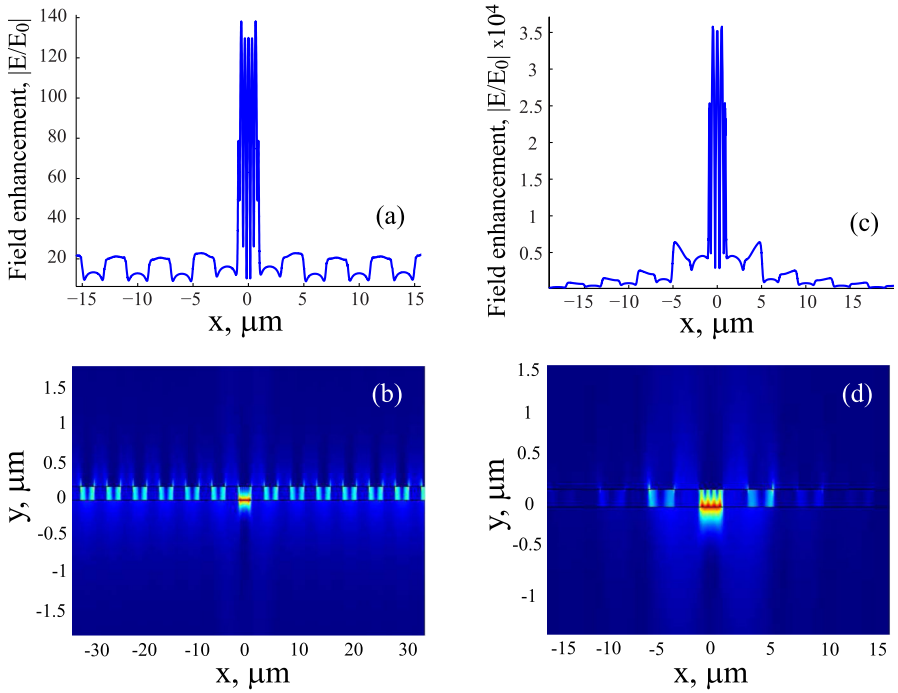

FIG. 4 (color online). (a) Normalized electric-field profile in the 2D electron channel and (b) maps of the electric-field distribution in the (x-y) plane for $\tau = 10^{-11}$ s; (c),(d) the same as in (a) and (b) for $\tau = 10^{-10}$ s.

plasmon excitations in the lattice unit cells adjacent to the cavity are suppressed. With increasing the lateral distance from the cavity, the plasmon energy in the lattice cell saturates at the level corresponding to the lattice plasmon resonance, see Fig. 3(c). This is due to the fact that the cavity mode is strongly pumped by the resonantly excited lattice plasmons. The Q factor of the resonances is about 20–30 for a electron scattering time $\tau = 10^{-11}$ s, achievable in highly purified heterostructures [27] and in graphene [28] at room temperatures.

We have also studied THz near-field enhancement for longer electron scattering time $\tau = 10^{-10}$ s (electron mobility $\mu \sim 10^6$ cm^2/V s), i.e., for lower losses. Such values of electron mobility can be achieved in semiconductor quantum wells at cryogenic temperatures [29], or in suspended graphene at room temperature [12]. In this case, the Q factor is much higher up to 3000 and hence the interaction between the cavity and the lattice plasmon modes is much stronger leading to a dramatic THz near-field enhancement factor $|\mathbf{E}/\mathbf{E}_0| \simeq 10\,000$, see Figs. 4(c) and 4(d), which, to the best of our knowledge, is much greater than any of the previously reported values [7,8]. Our calculations show that such dramatic enhancement of THz near field by 2D plasmons can be achieved at higher THz frequencies (up to several THz) in the structure with a smaller grating-gate period and a submicron plasmonic cavity.

In conclusion, we have studied THz field enhancement in the planar plasmonic crystal formed by a splt-grating-gate FET structure with a defect induced by an individually biased central finger. We have shown that the interaction between the cavity and the lattice plasmon modes can be electrically tuned by the voltage applied to the central gate finger. We predict an unprecedented THz electric-field enhancement factor up to 10 000 with a deep subwavelength concentration of the THz electric field. We believe that such strong THz electric-field enhancement can be utilized for THz nonlinear applications and for the design of the next generation of THz plasmonic devices.

We thank Dr. A. E. Miroshnichenko and Dr. O. V. Polischuk for useful discussions. This work has been supported by the Russian Foundation for Basic Research (Grants No. 10-02-93120 and 11-02-92101), by the Russian Academy of Sciences Program "Fundamentals of Nanotechnology and Nanomaterials," and by the Grant of the Government of the Russian Federation for supporting scientific research projects supervised by leading scientists at Russian institutions of higher education (Contract No. 11.G34.31.0030).

[1] X.-C. Zhang and J. Xu, *Introduction to THz Wave Photonics* (Springer-Verlag, New York, 2009).
[2] M. Tonouchi, Nature Photon. **1**, 97 (2007).
[3] T. D. Nguyen, Z. V. Vardeny, and A. Nahata, Opt. Express **18**, 25441 (2010).
[4] A. Rusina, M. Durach, K. A. Nelson, and M. I. Stockman, Opt. Express **16**, 18 576 (2008).
[5] M. Schnell, P. Alonso-Gonzalez, L. Arzubiaga, F. Casanova, L. E. Hueso, A. Chuvilin, and R. Hillebrand, Nature Photon. **5**, 283 (2011).

[6] H. Zhan, R. Mendis, and D. M. Mittleman, Opt. Express **18**, 9643 (2010).
[7] A. J. L. Adam, J. Infrared Millim. Terahz. Waves **32**, 976 (2011).
[8] M. A. Sao, H. R. Park, S. M. Koo, D. J. Park, J. H. Kang, O. K. Suwal, S. S. Choi, P. C. M. Planken, G. S. Park, N. K. Park, Q. H. Park, and D. S. Kim, Nature Photon. **3**, 152 (2009).
[9] C. R. Williams, S. R. Andrews, S. A. Maier, A. I. Fernadez-Dominguez, L. Martin-Moreno, and F. J. Garcia-Vidal, Nature Photon. **2**, 175 (2008).
[10] J. Lee, K. Lee, H. Park, G. Kang, D.-H. Yu, and K. Kim, Opt. Lett. **35**, 2254 (2010).
[11] K. S. Novoselov, A. K. Geim, S. V. Morozov, D. Jiang, Y. Zhang, S. V. Dubonos, I. V. Grigorieva, and A. A. Firsov, Science **306**, 666 (2004).
[12] F. Schwierz, Nature Nanotech. **5**, 487 (2010).
[13] W. Knap, S. Nadar, H. Videlier, S. Boubanga-Tombet, D. Coquillat, N. Dyakonova, F. Teppe, K. Karpierz, J. Lusakowski, M. Sakowicz, I. Kasalynas, D. Seliuta, G. Valusis, T. Otsuji, Y. Meziani, A. El Fatimy, S. Vandenbrouk, K. Madjour, D. Theron, and C. Gaquiere, J. Infrared Millim. Terahz. Waves **32**, 618 (2011).
[14] V. V. Popov, J. Infrared Millim. Terahz. Waves **32**, 1178 (2011).
[15] E. A. Shaner, M. Lee, M. C. Wanke, A. D. Grine, J. L. Reno, and S. J. Allen, Appl. Phys. Lett. **87**, 193507 (2005).
[16] E. A. Shaner, M. C. Wanke, A. D. Grine, S. K. Lyo, J. L. Reno, and S. J. Allen, Appl. Phys. Lett. **90**, 181127 (2007).
[17] A. Urich, K. Unterrainer, and T. Mueller, Nano Lett. **11**, 2804 (2011).
[18] T. J. Echtermeyer, L. Britnell, L. Jasnos, A. Lombardo, R. V. Gorbachev, A. N. Grigorenko, A. K. Geim, A. C. Ferrari, and K. S. Novoselov, Nature Commun. **2**, 458 (2011).
[19] F. Bonaccorso, Z. Sun, T. Hasan, and A. C. Ferrari, Nature Photon. **4**, 611 (2010).
[20] F. H. Koppens, D. E. Chang, and F. J. Garcia de Abajo, Nano Lett. **11**, 3370 (2011).
[21] A. Vakil and N. Engheta, Science **332**, 1291 (2011).
[22] L. A. Falkovsky and A. A. Varlamov, Eur. Phys. J. B **56**, 281 (2007).
[23] A. Hill, S. A. Mikhailov, and K. Ziegler, Europhys. Lett. **87**, 27005 (2009).
[24] Yu. Liu, R. F. Willis, K. V. Emtsev, and Th. Seyller, Phys. Rev. B **78**, 201403(R) (2008).
[25] V. V. Popov, O. V. Polischuk, and M. S. Shur, J. Appl. Phys. **98**, 033510 (2005).
[26] S. Fan, J. N. Winn, A. Devenyi, J. C. Chen, R. D. Meade, and J. D. Joannopoulos, J. Opt. Soc. Am. B **12**, 1267 (1995).
[27] G. Delhaye, L. Desplanque, and X. Wallart, J. Appl. Phys. **104**, 066105 (2008).
[28] J.-H. Chen, C. Jang, S. Xiao, M. Isigami, and M. S. Fuhrer, Nature Nanotech. **3**, 206 (2008).
[29] V. Umansky, M. Heiblum, Y. Levinson, J. Smet, J. Nubler, and M. Dolev, J. Cryst. Growth **311**, 1658 (2009).